

# Molecular Dynamics Simulations of the Growth Inhibiting Effect of $\text{Fe}^{2+}$ , $\text{Mg}^{2+}$ , $\text{Cd}^{2+}$ , and $\text{Sr}^{2+}$ on Calcite Crystal Growth

N. H. de Leeuw<sup>†</sup>

Department of Chemistry, University of Reading, Whiteknights, Reading RG6 6AD, U.K.

Received: December 10, 2001; In Final Form: February 11, 2002

Molecular dynamics simulations were employed to investigate the initial stages of growth of calcium, magnesium, iron, cadmium, and strontium carbonates at two experimentally observed calcite steps. The calculated energies suggest that in a solution containing all five cations  $\text{MgCO}_3$ ,  $\text{FeCO}_3$ , and  $\text{SrCO}_3$  grow onto the steps in preference to  $\text{CdCO}_3$  and especially  $\text{CaCO}_3$ . Initial incorporation of all impurity ions is more exothermic at the more open, obtuse step than at the acute step edge (by 44–86 kJ mol<sup>-1</sup>), although growth next to an existing  $\text{CaCO}_3$  unit occurs preferentially at the acute step. Growth of full rows of impurity carbonates is highly exothermic for the first row at -25 to -155 kJ mol<sup>-1</sup> per  $\text{MCO}_3$  depending on M (M = Mg, Fe, Cd, Sr), but is much less so for a subsequent row (-5 to -80 kJ mol<sup>-1</sup> per  $\text{MCO}_3$ ), due to increasing mismatch between the rows of  $\text{MCO}_3$  at the surface and the underlying calcite lattice, especially for the large strontium ion. Calcite growth, which is a slightly endothermic process in its pure form (on average +1.8 to +35 kJ mol<sup>-1</sup> per  $\text{CaCO}_3$ ), is severely hindered by the presence of impurity ions at the step edges, when the average enthalpies of the  $\text{CaCO}_3$  growth process increase to +15 to +75 kJ mol<sup>-1</sup> per  $\text{CaCO}_3$ , depending on the type of cation decorating the step. The results of these molecular dynamics simulations therefore suggest that growth of impurity carbonates at the calcite steps is initially an energetically very favorable process, hence competing effectively with growth of pure calcite. Subsequent incorporation of impurities, however, becomes more and more endothermic, until finally the presence of steps decorated with rows of impurities inhibits further crystal growth, in agreement with experimental evidence, which shows for example that the presence of magnesium and iron ions inhibits calcite growth.

## Introduction

Calcite is one of the most abundant minerals in the environment and of fundamental importance in many fields, both inorganic and biological. It is a building block of shells and skeletons<sup>1</sup> and is used as a carbon isotope counter in marine carbonates, with a view to assessing the relationship between the  $\text{CO}_2$ -induced greenhouse effect and climate.<sup>2</sup> Furthermore, calcium carbonate is important in ion exchange, due to its strong surface interactions with heavy metals in the environment,<sup>3,4</sup> in energy storage where the products of its endothermic decomposition into  $\text{CaO}$  and  $\text{CO}_2$  can be stored and subsequently reacted exothermically to re-release the energy,<sup>5</sup> and in industrial water treatment.<sup>6</sup> Hence, calcite has been the subject of extensive and varied research. One area of research that has attracted much attention is crystal growth and dissolution; see, e.g., refs 7–10. As the concentration of calcium carbonate in many natural waters exceeds the saturation level, the precipitation of calcite in industrial boilers, transportation pipes, and desalination plants is of concern,<sup>11</sup> and it is therefore important to learn how crystal growth and dissolution are affected and can be modified.

The  $\{10\bar{1}4\}$  surface is by far the most stable plane of calcite and dominates the observed morphology.<sup>12–14</sup> Hence, it has been the subject of many investigations, in ultrahigh vacuum such as the scanning electron microscopy study by Goni et al.,<sup>15</sup> in air,<sup>16</sup> and under aqueous conditions such as the atomic force microscopy (AFM) investigations by Ohnesorge and Binnig<sup>17</sup> and Liang et al.<sup>18</sup> However, no experimental surface is truly

planar and there are always defects present such as steps and kinks. Indeed, calcite growth and dissolution is found to occur through steps<sup>19</sup> and spiral dislocations,<sup>20</sup> often in monolayers from the step as observed by Liang et al. in their AFM study of the calcite  $\{10\bar{1}4\}$  plane under aqueous conditions<sup>18</sup> and by Stipp et al., who used SFM to study the same surface in air over some days and found the steps to spread one layer at a time.<sup>16</sup> In addition, side reactions, such as the oxidation of pyrite and ammonia, often affect the rate of  $\text{CaCO}_3$  dissolution.<sup>21</sup> Recent models of step dissolution have included a terrace-ledge-kink model, successfully describing the initial stages of pit growth on the  $\{10\bar{1}4\}$  surface,<sup>22,23</sup> a kinetic Monte Carlo model which reproduces experimental pit-growth behavior,<sup>24</sup> and molecular dynamics simulations, comparing dissolution of calcium carbonate units from two experimentally observed step edges, which correctly calculated the preference of dissolution from one particular step.<sup>25</sup>

Many impurity ions are found to affect crystal growth; e.g., Compton and Brown showed that magnesium ions inhibit calcite growth,<sup>26</sup> and hence studies of crystal growth have often concentrated on the effect of incorporating into the crystal foreign ions such as copper and manganese,<sup>27</sup> iron<sup>28</sup> and other divalent cations,<sup>29,30</sup> phosphate species,<sup>6,31</sup> or organic matter.<sup>32–34</sup> Earlier computational studies<sup>35,36</sup> have confirmed experimental findings<sup>37</sup> that lithium and  $\text{HPO}_4^{2-}$  impurities radically change the morphology of calcite, and predicted that magnesium ions would do likewise. Foreign ions can be incorporated at the growing steps, e.g., boron oxyanions,<sup>38</sup> and atomistic simulation methods have been used to model growth inhibition by incorporation of diphosphates into the steps.<sup>39</sup>

<sup>†</sup> E-mail: n.h.deleeuw@reading.ac.uk.

The aim of the work described in this paper is to use molecular dynamics (MD) simulations to investigate the enthalpies of the uptake of iron, magnesium, cadmium, and strontium ions into the growing calcite crystal. Iron, magnesium, cadmium, and strontium are all found as impurity ions in calcite, especially magnesium, which forms a complete solid solution with calcium from the purely isomorphous magnesium phase magnesite ( $\text{MgCO}_3$ ), through dolomite  $\text{CaMg}(\text{CO}_3)_2$ , which has an ordered 50/50 mixture of magnesium and calcium, to pure calcite.<sup>40</sup> Other carbonates also form solid solutions, such as siderite ( $\text{FeCO}_3$ ) with magnesite and to a lesser extent calcite.<sup>40</sup> The simulation of impurity uptake into the crystal is achieved by modeling the growth of  $\text{MgCO}_3$ ,  $\text{FeCO}_3$ ,  $\text{CdCO}_3$ , and  $\text{SrCO}_3$  units onto two experimentally observed monatomic steps on the calcite (10 $\bar{1}$ 4) surface. As crystal growth occurs under aqueous conditions, we have included solvent effects in the simulation by modeling the growth process in the presence of water molecules.

## Theoretical Methods

**Computational Techniques.** The energies of incorporation of iron, magnesium, cadmium, and strontium ions at the calcite surfaces were modeled using classical molecular dynamics simulations. These methods are based on the Born model of solids,<sup>41</sup> which assumes that the ions in the crystal interact via long-range electrostatic forces and short-range forces, including both the repulsions and the van der Waals attractions between neighboring electron charge clouds, which are described by simple analytical functions. The electronic polarizability of the ions is included via the shell model of Dick and Overhauser,<sup>42</sup> in which each polarizable ion, in our case the oxygen ion, is represented by a core and a massless shell, connected by a spring. The polarizability of the model ion is then determined by the spring constant and the charges of the core and shell. When necessary, angle-dependent forces are included to allow directionality of bonding as, for example, in the model of the covalent carbonate anion developed by Pavese et al.,<sup>43</sup> which is used in this work.

The computer code used for the molecular dynamics simulations was DL\_POLY 2.9.<sup>44</sup> To obtain the necessary data on bulk liquid water, a box containing 256 water molecules was simulated at a temperature of 300 K. The equilibration of the water simulation cell was achieved by initially setting the experimental density of  $\rho = 1.0 \text{ g/cm}^3$  and using NVE (constant number of particles, volume, and energy), NVT (constant number of particles, volume, and temperature), and NPT (constant number of particles, pressure, and energy) ensembles in sequence. The data collection simulations were run at NPT, where the final density was calculated at  $1.30 \text{ g/cm}^3$ .<sup>45</sup> Although larger than the experimental density of liquid water, the condensation energy was calculated at  $-42.7 \text{ kJ mol}^{-1}$ , which is in excellent agreement with the experimental value of  $-43.4 \text{ kJ mol}^{-1}$ .<sup>46</sup> The energies of the aqueous ions were calculated using a simulation cell containing 255 water molecules plus the cation or carbonate group. The simulation cell was equilibrated at NPT and 300 K for 10 000 time steps of 0.2 fs, after which data were collected for another 50 000 time steps. Then, comparing the average energy of this simulation cell with the energies of the 255 water molecules without the dissolved ion plus the energy of the isolated ion gave the energy of the hydrated ion. The stepped calcite surfaces were modeled as a repeating calcite slab, containing 120  $\text{CaCO}_3$  and  $\text{MCO}_3$  units and a gap containing the water molecules. The system was then simulated under NVT conditions for 100 ps per MD simulation.

Two different calcite surfaces were considered, and the simulation cells, consisting of calcite slab and 48 water molecules, contained 1152 species including shells. The cell dimensions were  $20 \text{ \AA} \times 25 \text{ \AA} \times 35 \text{ \AA}$  with a slab thickness of  $15 \text{ \AA}$  and water monolayers of  $3 \text{ \AA}$  depth.

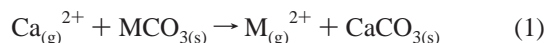
In the DL\_POLY code the integration algorithms are based around the Verlet leapfrog scheme,<sup>47</sup> and we used the Nosé–Hoover algorithm for the thermostat,<sup>48,49</sup> as this algorithm generates trajectories in both NVT and NPT ensembles, thus keeping our simulations consistent. The Nosé–Hoover parameters were set at 0.5 ps for both the thermostat and barostat relaxation times. There are two ways of treating the shells that are essentially massless: either performing an energy minimization of shells only at each time step<sup>50</sup> or assigning a small mass to the shells.<sup>51,52</sup> The latter is the approach used by DL\_POLY. We chose 0.2 au for the oxygen shell, which is small compared to the mass of the hydrogen atom of 1.0 au, which ensured that there would be no exchange of energy between vibrations of oxygen core and shell with oxygen and hydrogen vibrations.<sup>45</sup> However, due to the small shell mass we needed to run the MD simulations with a small time step of 0.2 fs to keep the system stable.

**Potential Model.** Calcite has a rhombohedral crystal structure with space group  $R\bar{3}c$  and  $a = b = 4.990 \text{ \AA}$ ,  $c = 17.061 \text{ \AA}$ ,  $\alpha = \beta = 90^\circ$ , and  $\gamma = 120^\circ$ .<sup>40</sup> We used the parameters for the short-range interactions derived empirically by Pavese et al. in their study of the thermal dependence of structural and elastic properties of calcite<sup>43</sup> to model the calcite crystal, and on static energy minimization we obtained a relaxed structure of  $a = b = 4.797 \text{ \AA}$ ,  $c = 17.482 \text{ \AA}$ ,  $\alpha = \beta = 90^\circ$ , and  $\gamma = 120^\circ$ . Although Pavese et al.'s potential model was fitted to bulk properties, it is generally possible for ionic materials to transfer potential parameters to surface calculations. In semiconductors, where the surface involves breaking bonds, and metals where the surface means a sudden change in the electron density, there is often a problem with transferability from bulk potential parameters to surfaces. However, in ionic materials after relaxation, the Madelung potentials are 90% or more of the bulk values and hence the change of ionic radii is negligible. Oliver et al.,<sup>53</sup> for example, used bulk derived potentials to model  $\text{WO}_3$  surfaces and found excellent agreement between their calculated and experimental surface structures, obtained by scanning tunneling microscopy. Since the surfaces considered in this work leave the carbonate group intact, the bulk derived potential model will be adequate. In addition, we showed in a previous study of the surface structures and stabilities of three calcium carbonate polymorphs, namely calcite, aragonite, and vaterite, that the potential model derived by Pavese et al. for calcite is directly transferable to different calcium carbonate phases, accurately reproducing the experimental morphologies of all three polymorphs.<sup>54</sup>

The potential models for  $\text{MgCO}_3$ ,  $\text{FeCO}_3$ , and  $\text{CdCO}_3$  were derived to be compatible with the aforementioned calcite potential model by Pavese et al.,<sup>43</sup> by fitting the parameters to reproduce the relative  $\text{MgCO}_3$ ,  $\text{FeCO}_3$ , and  $\text{CdCO}_3$  unit cell volumes with respect to calcite, and hence keep the experimental ratio of  $\text{Ca}:\text{Cd}:\text{Fe}:\text{Mg} = 1.32:1.22:1.05:1$ , which is identical with the ratio of the ionic radii of the different cations.<sup>55</sup> Strontianite ( $\text{SrCO}_3$ ), space group  $Pmcn$ , is isostructural with the aragonite phase rather than the calcite phase of  $\text{CaCO}_3$ , due to the larger size of the strontium ion. The  $\text{SrCO}_3$  potential model was therefore derived in a similar way to the  $\text{FeCO}_3$ ,  $\text{MgCO}_3$ , and  $\text{CdCO}_3$  potential parameters, but relative to the aragonite structure. The  $\text{SrCO}_3$  potential parameters are fitted to reproduce

the experimentally found relative cell volumes of Sr:Ca = 1.14:1 (from ref 40).

In addition to reproducing the structural parameters adequately, if we are to obtain reliable energies for growth of MgCO<sub>3</sub>, FeCO<sub>3</sub>, CdCO<sub>3</sub>, and SrCO<sub>3</sub> onto calcite, we require the relative energies of formation of the carbonates to be sensible. Hence, we required the enthalpies of the following reaction to be reproduced accurately:



where M is Mg, Fe, Cd, or Sr. The potential parameters were therefore derived, such that the calculated enthalpies of reaction 1 agree to within 8 kJ mol<sup>-1</sup> with the experimental enthalpies (<3.5% discrepancy).<sup>56,57</sup> Again, for SrCO<sub>3</sub> the reaction enthalpy of the process described in eq 1 was calculated relative to the aragonite phase.

The potential parameters used for the intra- and intermolecular water interactions are those described in a previous paper of MD simulations on MgO surfaces.<sup>45</sup> For the interactions between water molecules and calcite surfaces, we used the potential parameters previously fitted to calcite<sup>58</sup> and successfully used in MD simulations of water adsorption at point defects and crystal dissolution from calcite steps.<sup>25,59</sup> These potential parameters reproduce the experimental heat of formation of calcite from its aqueous ions to an acceptable degree of accuracy (within 20 kJ mol<sup>-1</sup>). In addition, good agreement was found between the experimental and calculated structural parameters of a crystalline calcium carbonate hexahydrate, ikaite (CaCO<sub>3</sub>·6H<sub>2</sub>O),<sup>58</sup> while the calculated change in enthalpy for the dissociation of ikaite into calcite and water was 47 kJ mol<sup>-1</sup> per water molecule compared to experimental values of 47–50 kJ mol<sup>-1</sup>,<sup>60</sup> again in excellent agreement even though the parameters were not fitted to this process. As the subject of this study is the replacement of calcium by impurity cations onto the growing calcite steps, the potential parameters for MgCO<sub>3</sub>, FeCO<sub>3</sub>, CdCO<sub>3</sub>, and SrCO<sub>3</sub> were also fitted to reproduce accurately (to within 12 kJ mol<sup>-1</sup>)<sup>61</sup> the experimental enthalpies of the following reaction:



where M is Mg, Fe, Cd, or Sr. Table 1 lists the parameters of the complete potential model used in this simulation study, while a comparison of calculated and experimental parameters for the various carbonates is made in Table 2.

## Results

Figure 1. shows the experimental crystal morphology of calcite, which is completely bounded by (1014) surfaces. These (1014) planes join each other at two different angles, either an acute angle or an obtuse angle. In this paper the effect of incorporation of impurity cations on calcite crystal growth is investigated. As calcite growth often occurs at monatomic steps,<sup>16,18</sup> the (3148) and (31216) vicinal surfaces were studied, which each contain planes of the dominant (1014) surface of calcite, offset from each other by monatomic steps. The sides of these steps are also (1014) surfaces, and the step edges of the two stepped surfaces, shown in Figure 2, are identical with the two different edges of the calcite rhomb joining at the same acute or obtuse angles as in the crystal morphology. The steps on the (3148) surface are acute; i.e. the carbonate groups on the edge of the step overhang the plane below the step and the angle between step wall and plane is 80° on the relaxed surface

**TABLE 1: Potential Parameters Used in This Work (short-range cutoff 10.10 Å)**

ion	charge ( <i>e</i> )		core–shell interaction (eV Å <sup>−2</sup> )
	core	shell	
Fe, Mg, Ca, Cd, Sr	+2.000		
C	+1.135		
H	+0.400		
carbonate oxygen (O)	+0.587	−1.632	507.400 000
water oxygen (Ow)	+1.250	−2.050	209.449 602
Buckingham Potential			
ion pair	<i>A</i> (eV)	<i>ρ</i> (Å)	<i>C</i> (eV Å <sup>6</sup> )
Ca–O	1 550.0	0.297 00	0.0
Ca–Ow	1 186.6	0.297 00	0.0
Fe– O	14 600.0	0.205 50	0.0
Fe–Ow	1 177.0	0.203 50	0.0
Mg–O	1 092.2	0.279 26	0.0
Mg–Ow	2 290.0	0.220 00	0.0
Cd–O	747 097.4	0.154 90	0.0
Cd–Ow	3 850.0	0.215 00	0.0
Sr–O	1 153.5	0.322 00	0.0
Sr–Ow	983.1	0.274 00	0.0
H–O	396.3	0.230 00	0.0
H–Ow	396.3	0.250 00	10.0
O–O	16 372.0	0.213 00	3.47
O–Ow	12 533.6	0.213 00	12.09
Lennard-Jones Potential			
	<i>A</i> (eV Å <sup>12</sup> )	<i>B</i> (eV Å <sup>6</sup> )	
Ow–Ow	39 344.98	42.15	
Morse Potential			
	<i>D</i> (eV)	<i>α</i> (Å <sup>−1</sup> )	<i>r</i> <sub>0</sub> (Å)
C–O <sub>core</sub>	4.710 000	3.800 00	1.180 00
H–Ow <sub>shell</sub>	6.203 713	2.220 03	0.923 76
Three-Body Potential			
	<i>k</i> (eV rad <sup>−2</sup> )	<i>Θ</i> <sub>0</sub>	
O <sub>core</sub> –C–O <sub>core</sub>	1.690 00	120.000 000	
H–Ow <sub>shell</sub> –H	4.199 78	108.693 195	
Four-Body Potential			
	<i>k</i> (eV rad <sup>−2</sup> )	<i>Θ</i> <sub>0</sub>	
C–O <sub>core</sub> –O <sub>core</sub> –O <sub>core</sub>	0.112 90	180.0	
Coulombic Subtraction (%)			
H <sup>0.4+</sup> –O <sup>0.8−</sup>		50	
H <sup>0.4+</sup> –H <sup>0.4+</sup>		50	

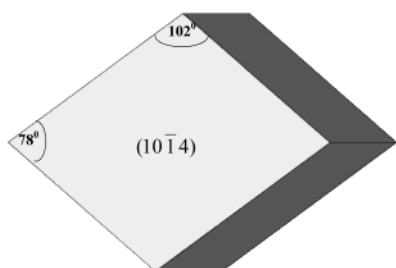
(cf. experimental value of 78°).<sup>4</sup> The steps on the (31216) surface on the other hand are obtuse; i.e. the carbonate groups on the step edge lean back with respect to the (1014) plane below with an angle between step wall and plane of 105° on the relaxed surface (experimental value 102°).<sup>4</sup> These two types of step are found experimentally to form the edges of etch pits,<sup>4,22</sup> and both dissolution and growth are found to occur from the step edges.

To model aqueous conditions, the stepped surfaces were covered in a monolayer of water molecules, one per surface calcium atom, which is the preferred configuration for the calcite (1014) surface.<sup>58,59</sup> Previous molecular dynamics simulations of MgO surfaces in liquid water showed that there is a distinct difference in structure and density between the adsorbed monolayer and the bulk water,<sup>45</sup> and one adsorbed monolayer of water was found to be sufficient to mimic solvent effects and give results on calcite dissolution in good agreement with experiment.<sup>25</sup> In previous work, dissolution of calcite steps was modeled, calculating the process for unhydrated and hydrated



**TABLE 2: Calculated and Experimental Properties of Calcite ( $\text{CaCO}_3$ ), Magnesite ( $\text{MgCO}_3$ ), Siderite ( $\text{FeCO}_3$ ), Otavite ( $\text{CdCO}_3$ ), and Strontianite ( $\text{SrCO}_3$ )**

property	$\text{CaCO}_3$	$\text{MgCO}_3$	$\text{FeCO}_3$	$\text{CdCO}_3$	$\text{SrCO}_3$
$c/a$	3.64 (3.42)	3.42 (3.24)	3.47 (3.27)	3.60 (3.31)	1.23 (1.18)
$\Delta H_{\text{eq}1}$ (kJ mol <sup>-1</sup> )		304.9 (311.5)	-348.0 (-357.7)	249.4 (241.3)	119.6 (122.0)
$\Delta H_{\text{eq}2}$ (kJ mol <sup>-1</sup> )		23.3 (35.2)	9.0 (12.6)	-17.8 (-10.6)	-5.8 (-10.1)

**Figure 1.** (a) Experimental rhombohedral calcite morphology, bounded by (1014) surfaces, joining at acute and obtuse angles.

steps, where it was found that only when water was included in the calculations did the calculated results agree with experimental findings.<sup>25</sup> Because carbonate crystal growth occurs under sedimentary conditions, only growth and impurity incorporation at hydrated calcite steps is considered in this work. The relaxed, hydrated steps are shown in Figure 2, from which it can be seen that the water molecules do not adsorb in a regular pattern onto the surfaces, unlike the planar (10 $\bar{1}4$ ) surface,<sup>58,59</sup> and that there is some relaxation of the ions on the surface and especially at the step edge, including rotation of the carbonate groups. Previous calculations have shown that the charge neutral steps are far enough apart (>10 Å) that interactions between the steps need not be taken into account when calculating the energies of the different processes.<sup>25</sup>

**Growth of Pure Calcite.** Growth of pure calcite at the steps was considered first, simulating the addition of successive  $\text{CaCO}_3$  units to the growing edges and calculating the energy expended or released at each successive addition of a  $\text{CaCO}_3$  unit. The surfaces throughout were charge neutral, and neutral  $\text{CaCO}_3$  units were added to the surface, implying supersaturation conditions (at low concentrations charged units may adsorb). After addition of each  $\text{CaCO}_3$  unit, a full molecular dynamics simulation followed, whereby both the mineral surface and the adsorbed water molecules were allowed to relax to their new positions. Energies of growth of  $\text{CaCO}_3$  units at isolated positions on the two step edges were calculated, introducing one double and two single kink sites on each edge,<sup>23</sup> and also next to preadsorbed units, shown in Figure 3, where the energy values quoted are the energies required or released per calcium carbonate unit for each successive step. In all cases, growth next to an existing unit was found to be energetically more favorable as no new kink sites were then introduced at the step. Introduction of a single calcium carbonate unit at the obtuse step edge (+82 kJ mol<sup>-1</sup>) is much less energetically expensive than at the acute step (+123 kJ mol<sup>-1</sup>), and initial growth would therefore be expected to occur preferentially at the obtuse step. However, once the activation energy of incorporation of the initial unit has been overcome at the acute step edge and the kink sites have been created, it is energetically more favorable for further growth to occur at the acute step. Experimentally, calcite has been found to dissolve preferentially from the obtuse step edge,<sup>23</sup> which finding is supported if we consider the opposite process from Figure 3 (right to left in Figure 3). A much higher activation energy is calculated to be required to create the first kink sites at the dissolving acute edge

(+104 kJ mol<sup>-1</sup>) compared to the obtuse edge (+46 kJ mol<sup>-1</sup>).

MacInnis and Brantley measured an activation energy of approximately 37 kJ mol<sup>-1</sup> for the widening of microscopic etch pits,<sup>13</sup> which consist of pairs of the steps studied here, in reasonable agreement with the activation energy calculated here for the obtuse step. It is also suggestive that Liang and Baer<sup>23</sup> found a constant ratio of obtuse:acute dissolution velocity of approximately 2.3, while the acute:obtuse ratio of our calculated activation enthalpies of initial dissolution of the two steps is also 2.3. Calcite growth at the two monomolecular steps was studied by Gratz et al. using in situ AFM techniques.<sup>19</sup> They observed an obtuse:acute ratio of growth velocities at the steps of 1.5–2.25 depending on supersaturation. The ratio of activation enthalpies for initial growth of acute:obtuse calculated in this work is 1.5, which again agrees well with the ratio of growth velocities at high supersaturation (1.5) found by Gratz et al.<sup>19</sup> Although the good agreement between experimentally observed ratios of dissolution/growth velocities of the two steps and calculated (inverse) ratios of enthalpies of initial dissolution/growth may be fortuitous, it suggests that under supersaturated conditions the dissolution/growth process is thermodynamically driven and that these types of calculations may be useful in the prediction of trends in growth/dissolution velocities.

**Incorporation of Impurity Ions at Calcite Steps.** Having considered the stepwise growth of pure calcite at the acute and obtuse steps, the incorporation of successive  $\text{MCO}_3$  ( $\text{M} = \text{Mg}, \text{Fe}, \text{Cd}, \text{or Sr}$ ) units was next considered at the two steps, comparing the enthalpies of decorating the calcite steps with impurity cations. McLean proposed that the incorporation of impurity cations is governed by the reduction in elastic strain,<sup>62</sup> which is borne out for calcite by the experimental work of Sturchio et al., who found that large  $\text{Pb}^{2+}$  ions from solution are primarily incorporated on calcium sites in the surface atomic layer of calcite rather than in the bulk.<sup>63</sup> However, static energy calculations of the absorption of Mg and Cd at calcite surfaces and subsequent segregation into the bulk identified that the interactions of solvent with the surface ions is the determining factor when enthalpies of segregation are considered.<sup>56</sup> Those theoretical findings are borne out by experimental work on the incorporation of  $\text{Zn}^{2+}$  into the calcite lattice, where it was found that the zinc ions do not follow the ion size argument, which was suggested to be a result of strong interactions of  $\text{Zn}^{2+}$  with solvent molecules or specific surface sites.<sup>64</sup> Hence, when solvent is present, as in these MD simulations, the energetics of the process of impurity uptake at the calcite steps will be influenced by (i) the enthalpies of the reactions in eq 2, (ii) the reduction of elastic strain as proposed by McLean,<sup>62</sup> i.e., an ion size effect, and (iii) the relative strengths of the interactions between water and impurity ions at the surfaces compared to the calcium ions, which will affect the relaxation and hence the stability of the surfaces and their affinity for the impurity ions under consideration; see, e.g. ref 65.

Figure 4 shows the process for the addition of single  $\text{MCO}_3$  units at the two calcite steps, either isolated or at kink sites next to existing  $\text{CaCO}_3$  units. Unlike calcium, the incorporation of impurity carbonates at the growth steps is energetically favorable for all but initial cadmium at the acute step. Similarly

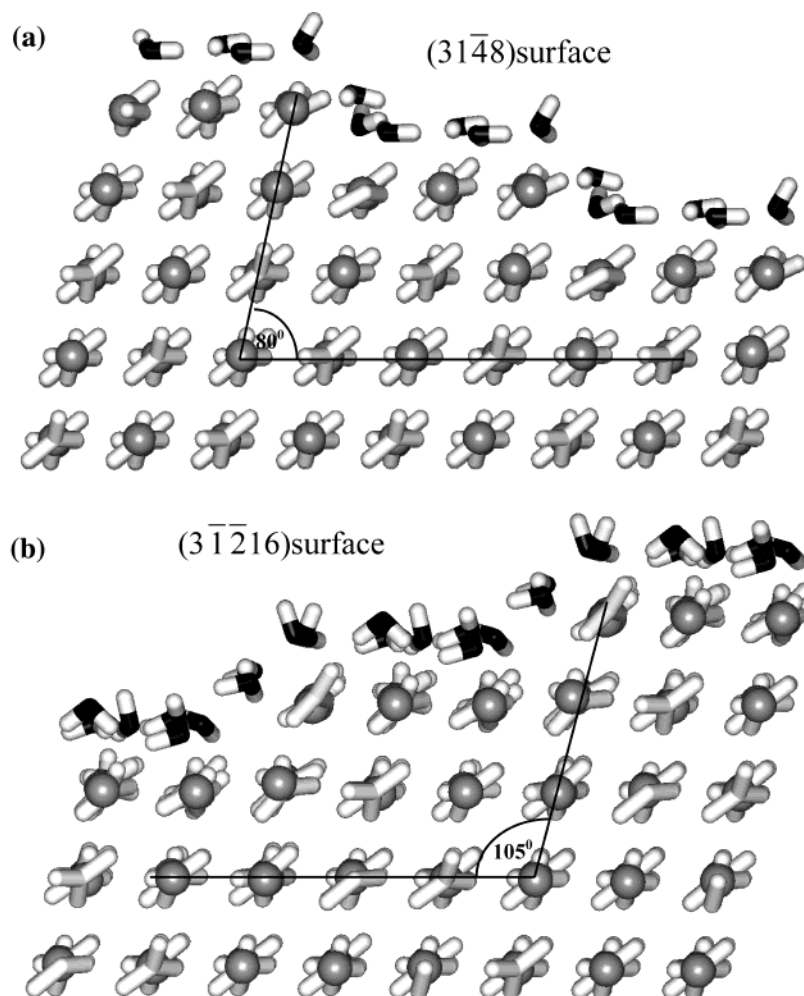


**Figure 2.** Side views of the calcite (3148) and (31216) surfaces, showing (1014) planes offset by (a) acute and (b) obtuse steps, with irregularly adsorbed water molecules (Ca = mid gray,  $\text{CO}_3$  = white,  $\text{O}_{\text{water}}$  = black, H = white).

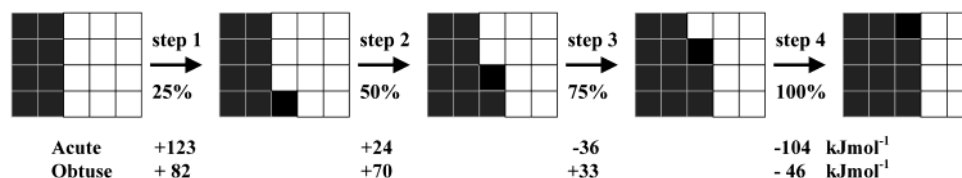


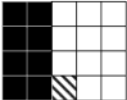
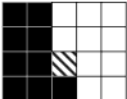
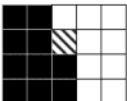
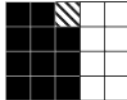
**Figure 3.** Schematic diagram of the energetics of incorporation of  $\text{CaCO}_3$  units at various growth sites on the acute and obtuse steps (top layer = black, second layer = white).

to calcium, the initial formation of kink sites and growth of the first  $\text{MCO}_3$  unit is more exothermic at the obtuse edge for all impurity ions, while addition at preexisting kink sites is more exothermic at the acute edge. Of the four impurity ions, iron is most easily incorporated at the growth steps, while the process of incorporating cadmium, which has an ionic radius similar to calcium, is the least favored, although still releasing large enthalpies when incorporated next to preexisting  $\text{CaCO}_3$  ions. Comparison to the energies of  $\text{CaCO}_3$  growth at the two step edges (Figure 3), which is an endothermic process in the initial stages, shows that even in the presence of a small amount of impurity cations, precipitation of  $\text{MCO}_3$  ( $\text{M} = \text{Mg}, \text{Fe}, \text{Cd}, \text{Sr}$ ) would be favored over pure  $\text{CaCO}_3$  on energetic grounds, in agreement with experimental investigations of the sorption of a variety of divalent metals on calcite, where it was found that significant sorption of impurity cations occurred at relatively low concentrations.<sup>66</sup>

As it is energetically favorable to incorporate single  $\text{MCO}_3$  units at the growth steps, the incorporation of additional impurity

carbonates was calculated next. Figure 5. shows the energies expended or released upon addition of successive  $\text{MCO}_3$  units ( $\text{M} = \text{Mg}, \text{Fe}, \text{Cd}, \text{Sr}$ ) at the acute and obtuse steps. Comparison with Figure 3 shows again that at all stages on both the acute and obtuse step edges addition of  $\text{CaCO}_3$  units, from the initial creation of kink sites up to formation of a full step, is energetically the least favorable process compared to incremental addition of  $\text{MgCO}_3$ ,  $\text{FeCO}_3$ ,  $\text{CdCO}_3$ , and  $\text{SrCO}_3$ . However, a comparison of the energies of growing a full impurity edge (Figure 5) with growth of isolated impurity units next to calcium carbonate positions (Figure 4) shows that larger energies are released for the incorporation of isolated impurities next to existing calcium carbonate units than next to impurity units. However, as consecutive growth of impurities along the edges is exothermic, while growth of calcium carbonates next to impurities is endothermic, the formation of complete impurity decorated edges is a thermodynamically feasible process.

Once an impurity decorated step has been created, the next process considered is the addition of another row at the step

	Acute	Obtuse
		
Position 1		
		
Position 2		
		
Position 3		
		
Position 4		

Mg	-19	-65
Fe	-80	-166
Cd	+41	-10
Sr	-48	-92

Mg	-123	-101
Fe	-152	-191
Cd	-75	-48
Sr	-140	-92

Mg	-148	-104
Fe	-203	-152
Cd	-89	-48
Sr	-193	-128

Mg	-205	-188
Fe	-261	-205
Cd	-147	-113
Sr	-195	-154

**Figure 4.** Schematic diagram of the energetics of incorporation of  $\text{MCO}_3$  units (hashed boxes) ( $\text{M} = \text{Mg}, \text{Fe}, \text{Cd}, \text{Sr}$ ) at various growth sites on the acute and obtuse calcite steps (calcite top layer = black, impurity = hashed, second layer = white).

edge, of either more impurity carbonate units or calcium carbonate units, which processes are shown in Figures 6 and 7, respectively. When comparing Figure 6, where a second impurity row is calculated, with Figure 5, which shows the energies released on the incorporation of the first row of impurities, it is clear that much smaller energies are released upon addition of the second row of impurities. Indeed, for cadmium and strontium the initial addition of the  $\text{MCO}_3$  unit at the edge, entailing creation of the kink sites, is endothermic at both the acute and obtuse steps. Only the initial incorporation of the smaller magnesium and iron carbonate units at the obtuse step is still exothermic. There are two contributions to the enthalpies of incorporation of impurities in the calcite lattice. First, growing second and further impurity rows will lead to an increasing mismatch between the impurity carbonate units and the underlying calcite surface. In addition, the interactions of the surface cations with the adsorbing water molecules also play a role. The smaller cations iron and magnesium are still fairly easily incorporated in the calcite lattice, and the strong interactions between especially these cations and water help to stabilize the surfaces, which was shown in previous work for a number of magnesium-covered calcite surfaces.<sup>65</sup>

However, the most significant interactions between impurity ions and water molecules are formed at the edge of the step; hence addition of a new impurity row to an already existing one does not lead to extra interactions between the impurity cations and the water molecules, while the extra rows lead to a larger mismatch between impurity rows and the underlying calcite crystal. As a result, the incorporation of second impurity rows is not as exothermic as the first. Indeed, for the large strontium ion (Table 3 for ionic radii),<sup>55</sup> it is becoming increasingly difficult to be accommodated in the calcite lattice. For example, Figure 8 shows side and plane views of the average structure of the two complete strontium carbonate edges at the obtuse steps on the  $(3\bar{1}216)$  surface. The effect of the strontium ions is to disturb the cation lattice, which in the pure calcite remains very regular during the MD simulation (Figure 2), with the strontium ions forming a rumpled step edge. There is also

more disorder of the carbonate groups, especially at the edges where they rotate to accommodate the larger strontium ions.

As mentioned above, Figure 7 shows the energies of growing consecutive calcium carbonate units at the various impurity decorated steps. Comparison of these energies with those in Figure 3 shows that, in general, the growth of calcium carbonate at the impurity decorated step edges is an even more endothermic process than growth of pure calcite. Clearly, the presence of impurity ions, creating a mismatch between surface layer and the underlying lattice, has an inhibiting effect on calcite crystal growth.

## Discussion

Figure 9 shows plots of average growth energies per  $\text{MCO}_3$  unit for the two steps: (i) growing a complete edge of  $\text{MCO}_3$  onto the pure calcite steps; (ii) growing a second edge of impurity units on the impurity decorated steps; (iii) growing a  $\text{CaCO}_3$  edge on the steps decorated with impurity carbonate units. It is clear that growth of a complete row of calcium carbonate at both the acute and obtuse step is an energetically unfavorable process, which is made even more endothermic by the presence of rows of impurity ions (hashed blocks in Figure 9). Initial addition of a first row of impurities is an exothermic process for each cation studied, but addition of a second row is markedly less exothermic in each case, which suggests that growth of  $\text{MCO}_3$  at the steps will become an endothermic process after a few rows of impurities have been incorporated and addition of further impurity edges will be inhibited. As the presence of impurities has already inhibited the addition of further  $\text{CaCO}_3$  units, once impurity carbonates are also prevented from growing at the steps, further crystal growth under these supersaturation conditions will be severely hindered on energetic grounds.

Following the simple argument that the incorporation of impurity cations is governed by the reduction in elastic strain,<sup>62</sup> borne out for calcite by the work of Sturchio et al., who found that large  $\text{Pb}^{2+}$  ions from solution are primarily incorporated on calcium sites in the surface atomic layer of calcite,<sup>63</sup> we might expect to observe not only different growth energies for the various impurity ions considered, but also a tendency to absorb at different cation sites. Cadmium has an ionic radius similar to that of calcium (Table 3), and hence its incorporation into the calcite lattice should not induce any elastic strain. Figure 9 shows that on average incorporation of cadmium is approximately  $50\text{--}60 \text{ kJ mol}^{-1}$  per  $\text{CdCO}_3$  more exothermic than calcium. As the calculated enthalpy of reaction 2 for  $\text{CdCO}_3$  is  $-18 \text{ kJ mol}^{-1}$  per  $\text{CdCO}_3$ , this means that a further 30 (acute step) to  $40 \text{ kJ mol}^{-1}$  (obtuse step) per  $\text{CdCO}_3$  is due to extra relaxation of the cadmium ions at the two steps. On the basis of this size argument,  $\text{Mg}^{2+}$  and  $\text{Fe}^{2+}$  should be easily incorporated at both steps, although the process in eq 2 is endothermic for both cations ( $23.3$  and  $9.0 \text{ kJ mol}^{-1}$  respectively). Indeed, Figure 9 shows the process of incorporation of these small cations at both calcite steps to be highly exothermic, even for the growth of a second row of impurity carbonate units. On average, there is no preference by the  $\text{Mg}^{2+}$  or  $\text{Fe}^{2+}$  ions for either step, although it can be seen from Figure 5 that the first addition, creating the kink sites, is for both cations far more exothermic at the obtuse step than at the acute step. The configuration of the obtuse step, with the carbonate groups at an obtuse angle with the underlying plane, allows more relaxation around these isolated foreign cations than the acute step. However, the growth of subsequent  $\text{MgCO}_3$  and  $\text{FeCO}_3$  units is more exothermic at the acute step, as the less open

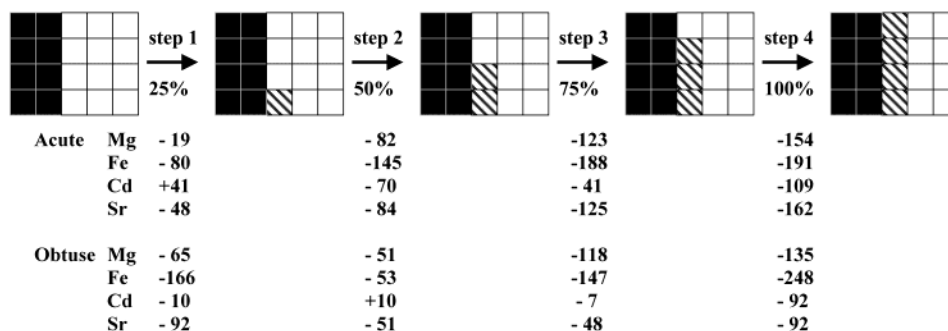


Figure 5. Schematic diagram listing the energies of successive additions of  $\text{MCO}_3$  units ( $\text{M} = \text{Mg}, \text{Fe}, \text{Cd}, \text{Sr}$ ) at the acute and obtuse calcite steps.

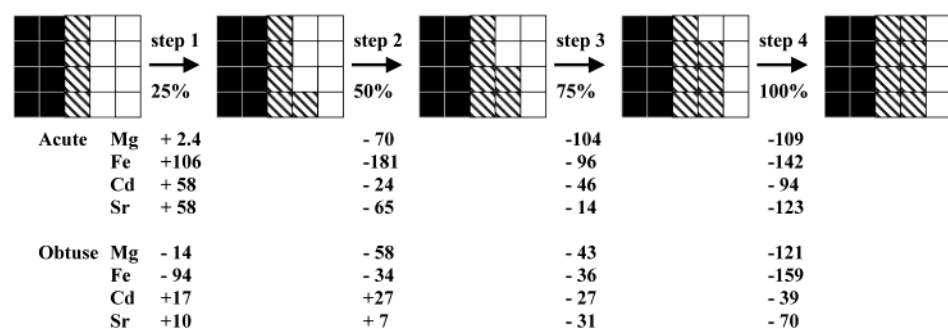


Figure 6. Schematic diagram listing the energies of addition of successive  $\text{MCO}_3$  units at the impurity decorated acute and obtuse calcite steps ( $\text{M} = \text{Mg}, \text{Fe}, \text{Cd}, \text{Sr}$ ).

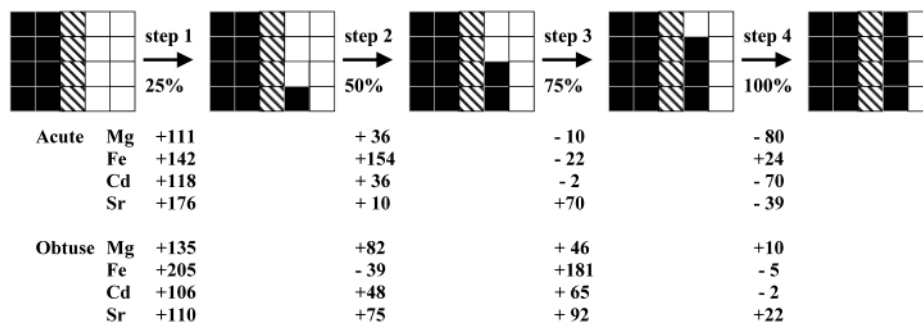


Figure 7. Schematic diagram listing the energies of addition of successive  $\text{CaCO}_3$  units at the impurity decorated acute and obtuse calcite steps.

TABLE 3: Ionic Radii of  $\text{Mg}^{2+}$ ,  $\text{Fe}^{2+}$ ,  $\text{Cd}^{2+}$ ,  $\text{Ca}^{2+}$ , and  $\text{Sr}^{2+}$

Mg	Fe	Cd	Ca	Sr
0.86	0.92	1.09	1.14	1.32

structure of this step is now more conducive for the incorporation of small cations at neighboring calcium sites, where the relaxation of the carbonate groups on the edge has to accommodate more than one impurity ion.

The enthalpy of eq 2 for  $\text{SrCO}_3$  is just exothermic, but the calculated value of  $-6 \text{ kJ mol}^{-1}$  per  $\text{SrCO}_3$  does not explain the large average energies released on growing strontium carbonate units at the two steps. As the ionic radius of strontium is considerably larger than that of calcium ( $\sim 16\%$ ), the strain induced in the lattice by the incorporation of strontium should be considerable. However, as the impurity ions are located at the edges of the steps, the surface ions can relax out of the surface, as was seen for example in Figure 8a, where rumpling of the surface strontium ions and rotation of the carbonate groups occurs. These extensive surface relaxations release the strain in the lattice, which would occur if strontium was introduced in the bulk calcite lattice. The larger average energy released upon addition of  $\text{SrCO}_3$  at the acute step, with its less open structure than the obtuse step, may seem anomalous, but comparison to the growth energies of the pure calcite at both steps shows that growth of  $\text{SrCO}_3$  is more exothermic by exactly

the same amount of  $107 \text{ kJ mol}^{-1}$  at both steps, while the addition of the initial  $\text{SrCO}_3$  unit again occurs at the obtuse step. Furthermore, when the second row of  $\text{SrCO}_3$  is added to the steps, the growth energies of  $\text{SrCO}_3$  decrease by approximately 70% for both steps, which is larger than any of the other impurity cations, due to the increase in mismatch between the stepped surface layer, largely consisting of  $\text{SrCO}_3$ , and the underlying calcite lattice.

There have been a number of experiments on the incorporation of impurities in growth hillocks on the  $(10\bar{1}4)$  surface.<sup>19,64,67,68</sup> The vicinal surfaces of these hillocks have directions  $[\bar{4}41]$  and  $[48\bar{1}]$ . Both the  $(3\bar{1}216)$  and  $(3148)$  surfaces are in the zone defined by the  $[\bar{4}41]$  direction and are therefore suitable vicinal surfaces to compare with these experimental investigations. X-ray fluorescence experiments show that a c-glide passes through the hillock, which relates the four vicinal surfaces into two pairs that incorporate different impurity ions. The experimental results find that ions with ionic radii smaller than  $\text{Ca}^{2+}$  are incorporated at smaller kink sites, corresponding to kink sites on our acute step, while the larger ions are incorporated at the more open kink site, corresponding to kink sites on our obtuse step. Our calculations, however, suggest that all the impurity ions considered here are preferably incorporated at the obtuse step, when no kink sites have as yet been created,



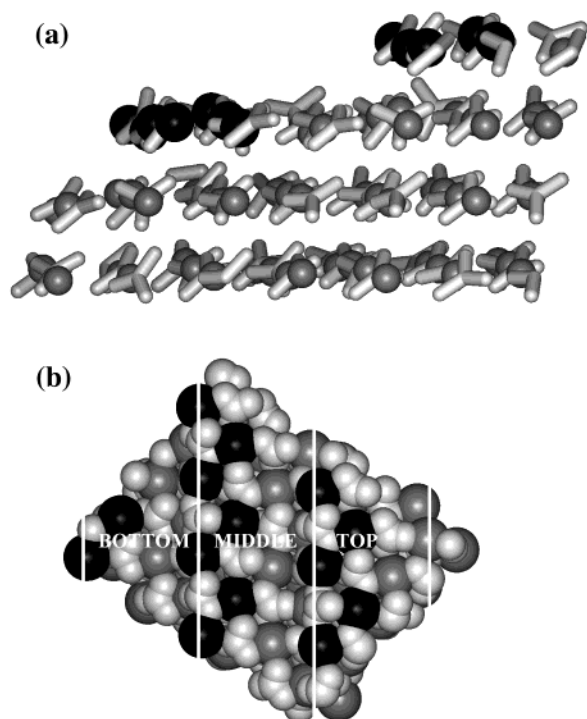


**Figure 8.** (a) Side and (b) plane view of the calcite ( $\bar{3}1\bar{2}16$ ) surface with obtuse steps decorated by two rows of  $\text{Sr}^{2+}$  ions, showing rumpling of the  $\text{Sr}^{2+}$  on the edges and distortion of the calcium lattice. The height of the different (1014) planes offset by the steps is indicated in (b) by "top, middle, and bottom" (Ca = mid gray, Sr = black,  $\text{CO}_3$  = white, water molecules not shown).

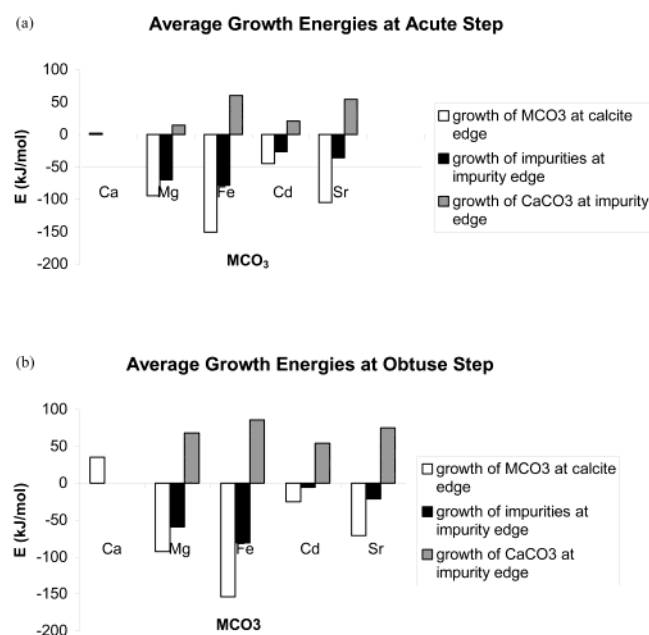


**Figure 9.** Bar charts of the average energies per  $\text{MCO}_3$  unit ( $\text{M} = \text{Ca}, \text{Mg}, \text{Fe}, \text{Cd}, \text{Sr}$ ) required or released upon the growth of a full  $\text{MCO}_3$  row at (a) the acute and (b) the obtuse calcite step, showing the increasing endothermicity of  $\text{CaCO}_3$  growth as a result of the incorporation of successive rows of impurity cations.

while they all prefer to be incorporated at the acute step edge, when the kink sites have already been introduced by a preabsorbed  $\text{CaCO}_3$  unit. However, the experimental measurements were analyzed in terms of a vacuum surface, while our calculations take into account the effect of solvent. Many previous studies have shown that the presence of water has a large effect on surface stabilities and adsorption energies of

impurities (e.g., refs 25, 54, 56, and 58), and solvent may well play a deciding role in the stabilization of the different kink sites for impurity incorporation.

## Conclusion

Molecular dynamics simulations of the initial stages of growth of calcium, magnesium, iron, cadmium, and strontium carbonate at two experimentally observed calcite steps suggest that in a solution containing all five cations,  $\text{MgCO}_3$ ,  $\text{FeCO}_3$ , and  $\text{SrCO}_3$  grow onto the steps in preference to  $\text{CdCO}_3$  and especially  $\text{CaCO}_3$ . Initial incorporation of all impurity ions is more exothermic at the obtuse step, although growth next to an existing  $\text{CaCO}_3$  unit occurs preferentially at the acute step. Growth of full rows of impurity carbonates is highly exothermic for the first row, but is much less so for a subsequent row, due to mismatch between the rows of  $\text{MCO}_3$  at the surface ( $\text{M} = \text{Mg}, \text{Fe}, \text{Cd}, \text{Sr}$ ) and the underlying calcite lattice, especially for the large strontium ion. Calcite growth, which is a slightly endothermic process in its pure form, is severely hindered by the presence of impurity ions at the step edges.

The results of these MD simulations therefore suggest that growth of impurity carbonates at the calcite steps is initially an energetically very favorable process, hence competing very effectively with growth of pure calcite, in agreement with experimental studies of the uptake of divalent impurity ions, which found that all ions investigated in this study would be incorporated into the calcite crystal.<sup>26,28,30,64,68</sup> Subsequent growth of impurities, however, becomes more and more endothermic, until finally the presence of steps decorated with rows of impurities inhibits further crystal growth. This suggestion is also borne out by experimental evidence, which shows for example that the presence of magnesium and iron ions inhibits calcite growth,<sup>26,28,30</sup> where the growth inhibition is found to increase with increasing ion concentration, e.g., ref 28.

**Acknowledgment.** N.H.L. thanks NERC (Grant NER/M/S/2001/00068), the Royal Society (Grant 22292), and the Wellcome Trust (Grant 065067) for financial support.

## References and Notes

- Beruto, D.; Giordani, M. *J. Chem. Soc., Faraday Trans.* **1993**, 89, 2457.
- Romanek, C. S.; Grossman, E. L.; Morse, J. W. *Geochim. Cosmochim. Acta* **1992**, 56, 419.
- Stipp, S. L.; Hochella, M. F. *Geochim. Cosmochim. Acta* **1991**, 55, 1723.
- Park, N.-S.; Kim, M.-W.; Langford, S. C.; Dickinson, J. T. *Langmuir* **1996**, 12, 4599.
- Chakraborty, D.; Bhatia, S. K. *Ind. Eng. Chem. Res.* **1996**, 35, 1995.
- Dove, P. M.; Hochella, M. F. *Geochim. Cosmochim. Acta* **1993**, 57, 705.
- Dreybolt, W.; Eisenlohr, L.; Madry, B.; Ringer, S. *Geochim. Cosmochim. Acta* **1997**, 61, 3897.
- Liu, Z.; Dreybolt, W. *Geochim. Cosmochim. Acta* **1997**, 61, 2879.
- Reeder, R. J.; Valley, J. W.; Graham, C. M.; Eiler, J. M. *Geochim. Cosmochim. Acta* **1997**, 61, 5057.
- Zuddas, P.; Mucci, A. *Geochim. Cosmochim. Acta* **1998**, 62, 757.
- Chakraborty, D.; Agarwal, V. K.; Bhatia, S. K.; Belare, J. *Ind. Eng. Chem. Res.* **1994**, 33, 2187.
- Blanchard, D. L.; Baer, D. R. *Surf. Sci.* **1992**, 276, 27.
- MacInnes, I. N.; Brantley, S. L. *Geochim. Cosmochim. Acta* **1992**, 56, 1113.
- Didymus, J. M.; Oliver, P. M.; Mann, S.; De Vries, A. L.; Hauschka, P. V.; Westbroek, P. *J. Chem. Soc., Faraday Trans.* **1993**, 89, 2891.
- Goni, S.; Sobrado, L.; Hernandez, M. S. *Solid State Ionics* **1993**, 63, 786.
- Stipp, S. L.; Gutmannsbauer, W.; Lehmann, T. *Am. Mineral.* **1996**, 81, 1.
- Ohnesorge, P.; Binnig, G. *Science* **1993**, 260, 1451.



- (18) Liang, Y.; Lea, A. S.; Baer, D. R.; Engelhard, M. H. *Surf. Sci.* **1996**, *351*, 172.
- (19) Gratz, A. J.; Hillner, P. E.; Hansma, P. K. *Geochim. Cosmochim. Acta* **1993**, *57*, 491.
- (20) Hillner, P. E.; Manne, S.; Hansma, P. K.; Gratz, A. J. *Faraday Discuss.* **1993**, *95*, 191.
- (21) Wilson, T. R. S.; Thomson, J. *Geochim. Cosmochim. Acta* **1998**, *62*, 2087.
- (22) Liang, Y.; Baer, D. R.; McCoy, J. M.; Amonette, J. E.; LaFemina, J. P. *Geochim. Cosmochim. Acta* **1996**, *60*, 4883.
- (23) Liang, Y.; Baer, D. R. *Surf. Sci.* **1997**, *373*, 275.
- (24) McCoy, J. M.; LaFemina, J. P. *Surf. Sci.* **1997**, *373*, 288.
- (25) de Leeuw, N. H.; Parker, S. C.; Harding, J. H. *Phys. Rev. B* **1999**, *60*, 13792.
- (26) Compton, R. G.; Brown, C. A. *J. Colloid Interface Sci.* **1994**, *165*, 445.
- (27) Nassralla-Aboukais, N.; Boughriet, A.; Fischer, J. C.; Wartel, M.; Langelin, H. R.; Aboukais, A. *J. Chem. Soc., Faraday Trans.* **1996**, *92*, 3211.
- (28) Katz, J. L.; Reick, M. R.; Herzog, R. E.; Parsiegl, K. J. *Langmuir* **1993**, *9*, 1423.
- (29) Brecevic, L.; Nothig-Laslo, V.; Kralj, D.; S. Popovic, S. *J. Chem. Soc., Faraday Trans.* **1996**, *92*, 1017.
- (30) Deleuze, M.; Brantley, S. L. *Geochim. Cosmochim. Acta* **1997**, *61*, 1475.
- (31) Suzuki, T.; Inomata, S.; Sawada, K. *J. Chem. Soc., Faraday Trans. I* **1986**, *82*, 1733.
- (32) Cicerone, D. S.; Regazzoni, A. E.; Blesa, M. A. *J. Colloid Interface Sci.* **1992**, *154*, 423.
- (33) Lebrón, I.; Suárez, D. L. *Geochim. Cosmochim. Acta* **1996**, *60*, 2765.
- (34) Lebrón I.; Suárez, D. L. *Geochim. Cosmochim. Acta* **1998**, *62*, 405.
- (35) Kenway, P. R.; Oliver, P. M.; Parker, S. C.; Sayle, D. C.; Sayle, T. X. T.; Titiloye, J. O. *Mol. Simul.* **1992**, *9*, 83.
- (36) Parker, S. C.; Kelsey, E. T.; Oliver, P. M.; Titiloye, J. O. *Faraday Discuss.* **1993**, *94*, 75.
- (37) Rajam, S.; Mann, S. *J. Chem. Soc., Chem. Commun.* **1990**, 1789.
- (38) Hemming, N. G.; Reeder, R. J.; Hart, S. R. *Geochim. Cosmochim. Acta* **1998**, *62*, 2915.
- (39) Nygren, M. A.; Gay, D. H.; Catlow, C. R. A.; Rohl, A. L.; Wilson, M. P. *J. Chem. Soc., Faraday Trans.* **1998**, *94*, 3685.
- (40) Deer, W. A.; Howie, R. A.; Zussmann, J. *Introduction to the Rock-forming Minerals*; Longman: Harlow, UK, 1992.
- (41) Born, M.; Huang, K. *Dynamical Theory of Crystal Lattices*; Oxford University Press: Oxford, 1954.
- (42) Dick, B. G.; Overhauser, A. W. *Phys. Rev.* **1958**, *112*, 90.
- (43) Pavese, A.; Catti, M.; Parker, S. C.; Wall, A. *Phys. Chem. Miner.* **1996**, *23*, 89.
- (44) Forester, T. R.; Smith, W. *DL\_POLY user manual*; CCLRC; Daresbury Laboratory: Daresbury, Warrington, UK, 1995.
- (45) de Leeuw, N. H.; Parker, S. C. *Phys. Rev. B* **1998**, *58*, 13901.
- (46) Duan, Z.; Moller, N.; Weare, J. H. *Geochim. Cosmochim. Acta* **1995**, *59*, 3273.
- (47) Verlet, L. *Phys. Rev.* **1967**, *195*, 98.
- (48) Nosé, S. *J. Chem. Phys.* **1984**, *81*, 511.
- (49) Hoover, W. G. *Phys. Rev. A* **1985**, *31*, 1695.
- (50) Lindan, P. J. D.; Gillan, M. J. *J. Phys.: Condens. Matter* **1993**, *5*, 1019.
- (51) Mitchell, P. J.; Fincham, D. *J. Phys.: Condens. Matter* **1993**, *5*, 1031.
- (52) Ferneyhough, R.; Fincham, D.; Price, G. D.; Gillan, M. J. *Model. Simul. Mater. Sci. Eng.* **1994**, *2*, 1101.
- (53) Oliver, P. M.; Parker, S. C.; Egdell, R. G.; Jones, F. H. *J. Chem. Soc., Faraday Trans.* **1996**, *92*, 2049.
- (54) de Leeuw, N. H.; Parker, S. C. *J. Phys. Chem. B* **1998**, *102*, 2914.
- (55) Shannon, R. D. *Acta Crystallogr., Sect. A* **1976**, *32*, 751.
- (56) de Leeuw, N. H.; Parker, S. C. *J. Chem. Phys.* **2000**, *112*, 4326.
- (57) Lide, D. R. *CRC Handbook of Chemistry and Physics*; CRC: Boca Raton, FL, 2000.
- (58) de Leeuw, N. H.; Parker, S. C. *J. Chem. Soc., Faraday Trans.* **1997**, *93*, 467.
- (59) de Leeuw, N. H.; Parker, S. C. *Mol. Simul.* **2000**, *24*, 71.
- (60) Bischoff, J. L.; Fitzpatrick, J. A.; Rosenbauer, R. J. *J. Geol.* **1993**, *101*, 21.
- (61) Weast R. C.; Astle, M. J. *CRC Handbook of Chemistry and Physics*; CRC: Boca Raton, FL, 1981.
- (62) McLean, D. *Grain Boundaries in Metals*; Clarendon Press: Oxford, 1957.
- (63) Sturchio, N. C.; Chiarello, R. P.; Cheng, L.; Lyman, P. F.; Bedzyk, M. J.; Qian, Y.; You, H.; Yee, D.; Geissbuhler, P.; Sorensen, L. B.; Liang, Y.; Baer, D. R. *Geochim. Cosmochim. Acta* **1997**, *61*, 251.
- (64) Reeder, R. J. *Geochim. Cosmochim. Acta* **1996**, *60*, 1543.
- (65) de Leeuw, N. H.; Parker, S. C. *Phys. Chem. Chem. Phys.* **2001**, *3*, 3217.
- (66) Zachara, J. M.; Cowan, C. E.; Resch, C. T. *Geochim. Cosmochim. Acta* **1991**, *55*, 1549.
- (67) Paquette, J.; Reeder, R. J. *Geology* **1990**, *18*, 1244.
- (68) Paquette, J.; Reeder, R. J. *Geochim. Cosmochim. Acta* **1995**, *59*, 735.